Available online at www.sciencedirect.com
ScienceDirect
International Journal of Heat and Mass Transfer 51 (2008) 1770–1779
International Journal of HEAT and MASS TRANSFER
www.elsevier.com/locate/ijhmt

A comparative study on poiseuille flow of simple fluids through cylindrical and slit-like nanochannels

X. Song, J.K. Chen *

Department of Mechanical and Aerospace Engineering, University of Missouri Columbia, Columbia, MO 65211, United States

Received 14 August 2006; received in revised form 6 July 2007
Available online 6 September 2007

Abstract

Poiseuille flow of simple fluids in cylindrical nanochannels is investigated by nonequilibrium molecular dynamics simulations. The effects of pore shape and size are studied by comparing the fluid behavior in cylindrical and slit-like pores. It is found that the cylindrical pores are involved with a stronger molecular interaction between the fluid and wall atoms due to larger surface-to-volume ratio, curvature and possibly greater molecular roughness. The fluid-wall interaction plays an important role in the fluid flow at nanoscale. As a result, the bulk fluid density in cylindrical pores is lower than in the slit-like pores because a larger number of fluid particles are apposed onto the wall surface. In addition, evident slip on the boundary is observed in the cylindrical pore while no slip occurs in the slit-like pore. The fluid in the cylindrical pores has lower temperature and more uniform temperature distribution. This suggests that the cylindrical pores perform better to conduct the viscous heat out of the channel than the slit-like pores.

Keywords: Poiseuille flow; Nanochannels; Molecular dynamics; Cylindrical pore; Slit-like pore

1. Introduction

The fluid flow subject to nanoscale confinement has demonstrated interesting phenomena, which cannot be described by the classical Navier–Stokes hydrodynamics [1–4]. It was found that the density of the fluid in the direction of confinement can vary appreciably, and the positional dependence of the fluid transport properties can become significant. Moreover, due to the large surface-to-volume ratios, the interaction between the fluid and confinement wall imposes innegligible influence on the structural and dynamical characteristics of the fluid. It has been demonstrated that molecular dynamics (MD) simulation is a powerful tool to investigate these complicated phenomena by including the unconventional effects such as slip flow, viscous dissipation, and intermolecular forces. The molecular dynamics study of these effects could provide information that is difficult to be obtained by experiments, and thereby improve our understanding in the technological processes such as flow in microporous media, and transport of biological and chemical materials through nanodevices or microdevices.

Most MD simulations of Poiseuille flow in narrow channels have focused on the fluid behavior in slit-like pores [3–13]. Travis et al. [3,4] carried out nonequilibrium molecular dynamics simulations of fluid flow in slit pores with the width of only a few molecular diameters. They have studied the structural and dynamic characteristics of the flow, including density, streaming velocity, temperature, viscosity, and thermal conductivity. The formation of fluid layers induced by fluid-wall interaction led to a non-uniform density profile. The velocity profiles were found to deviate from the continuum quadratic solution, but possess an underlying quadratic signature with superimposed oscillations. The authors proposed that it might

* Corresponding author. Tel.: +1 573 882 8159; fax: +1 573 884 5090.
E-mail address: Chenjnk@missouri.edu (J.K. Chen).

0017-9310/$ - see front matter © 2007 Elsevier Ltd. All rights reserved.
doi:10.1016/j.ijheatmasstransfer.2007.07.019

be possible to extend hydrodynamics into the regime by introducing the concept of nonlocal viscosity and a nonlocal form of constitutive relation, in which the stress is not proportional to the local strain rate, but depends on the entire field of the strain rate. Travis and his colleagues concluded from their results that the no slip boundary conditions were still valid even in the case that the fluid-wall interaction is governed by the repulsive Weeks–Chandler–Andersen potential. However, other researchers [1,5–11] observed the phenomenon of wall slip in their simulations, and found that the boundary condition at wall-fluid interface could depend on the interface wettability, the mangnitude of the driving force, and channel size.

Despite the similarities in macroscale flows in cylindrical and slit-like pores, the effect of different shape and surface-to-volume ratios could cause important differences in the transport of fluids at micro- or nano-scales. However, there has been relatively little work on fluid flow in cylindrical pores. Most of the previous works [14–17] were carried out to study the transport of molecules adsorbed in cylindrical pores, and the studies were generally more concerned with the fluids of low density. Sokhan et al. [18] simulated the steady-state Poiseuille flow of a simple fluid in carbon nanotubes. The molecular corrugation introduced by the surface of carbon nanotubes was found to be very low. Therefore, the carbon nanotubes were modeled as a smooth continuum of the tubular shape. The authors proposed appropriate hydrodynamics boundary conditions to model the lateral stresses imparted to the fluids by the carbon nanotube surfaces.

To understand the transport behavior of nanoscale flows in a cylindrical pore, we perform nonequilibrium molecular dynamics (NEMD) simulations for the gravity force driven Poiseuille flow of Lennard-Jones fluids through cylindrical pores of different sizes. Two types of models are used to represent the confinement of the pore walls. One is the structureless thermal wall, which controls the temperature in a stochastic manner and does not consider the molecular interaction between the fluid and wall. The other is the more realistic structured wall, which consists of several layers of solid wall molecules. The latter takes into account the interaction potential between fluid and solid wall molecules. Comparing the results of the two different wall models allows us to differentiate the effects of physical confinement and molecular forces imposed by wall molecules. The Poiseuille flows in the slit-like pores of the comparable sizes are also simulated. The fluid behaviors in the two different geometries are compared to study how the pore shape affects the structural and dynamical properties of the fluid at nanoscale.

The article is organized as follows. The next section describes the details of the NEMD simulations. In Section 3, the results of the simulations are presented and discussed. Concluding remarks follow in the last section.

2. Details of models and simulations

We consider a system of fluid particles interacting via the Lennard-Jones pairwise potential

$$\phi_f(d) = 4\varepsilon_f\left[\left(\frac{\sigma_f}{d}\right)^{12} - \left(\frac{\sigma_f}{d}\right)^{6}\right] \tag{1}$$

where d is the distance between a pair of particles, and σ_f and ε_f represent the characteristic length and energy scale of the interaction, respectively. In this study, $\sigma_f = 3.405$ Å and $\varepsilon_f = 1.67 \times 10^{-21}$ J. These are the values of the parameters for liquid argon. A common choice of the cut-off distance is 2.5 σ_f [19], outside of which atoms j makes only a small contribution (<1%) to the intermolecular force on the atom. For computational convenience, the length scale σ_f, the energy scale ε_f, and the atomic mass of the argon atom ($m_f = 6.63 \times 10^{-26}$ kg) are used to non-dimensionalize all the physical quantities. The characteristic time scale is thus defined as $\tau = \sigma_f\sqrt{m_f/\varepsilon_f}$, and equal to 2.16×10^{-12} s. The dimensionless atomic number density ρ^*, velocity $\bar{v}^*$, and temperature T^* are defined as follows:

$$\begin{aligned} \rho^* &= \rho\sigma_f^3 \\ \bar{v}^* &= \bar{v}\sqrt{m_f/\varepsilon_f} \\ T^* &= kT/\varepsilon_f \end{aligned} \tag{2}$$

where k is the Boltzmann constant.

Two types of models (thermal wall and structured wall) are used to represent the wall confinement. The thermal wall is a virtual surface and the fluid-wall interaction is simulated in a stochastic way. The structured wall is comprised of individual solid wall atoms and the interaction between the solid and fluid particles is also in the form of Lennard–Jones potential. The details of the thermal and structured wall models are given in Sections 2.1 and 2.2, respectively.

In the numerical study, we first carry out an equilibrium molecular dynamics simulation for a fluid with an initially assigned number density (ρ^*_{avg}) of 0.78, for which the number of atoms is about 10% more than that estimated based on the equilibrium position $2^{1/6}\sigma_f$. After the equilibrium state is achieved, the initial positions of the fluid particles for the NEMD simulation are obtained by cutting a block of argon atoms in either cylindrical or hexahedral shapes out of the bulk fluid. In a similar way, the pore walls are carved from the solid lattice for the structured wall system. Fig. 1 shows a diagram of the systems investigated. The fluid particles are bounded by the walls and subject to a constant external force (g) in the x direction, which has the same effect as allowing gravity to initiate the flow down the pores. Non-dimensional driving force ($g^* = g\sigma_f/\varepsilon_f$) takes the values of 0.5, 1.0, and 2.0. During flow, part of the work done by the external force is converted into heat and causes the continuous increase of the fluid temperature. To remove the heat and keep the temperature of the

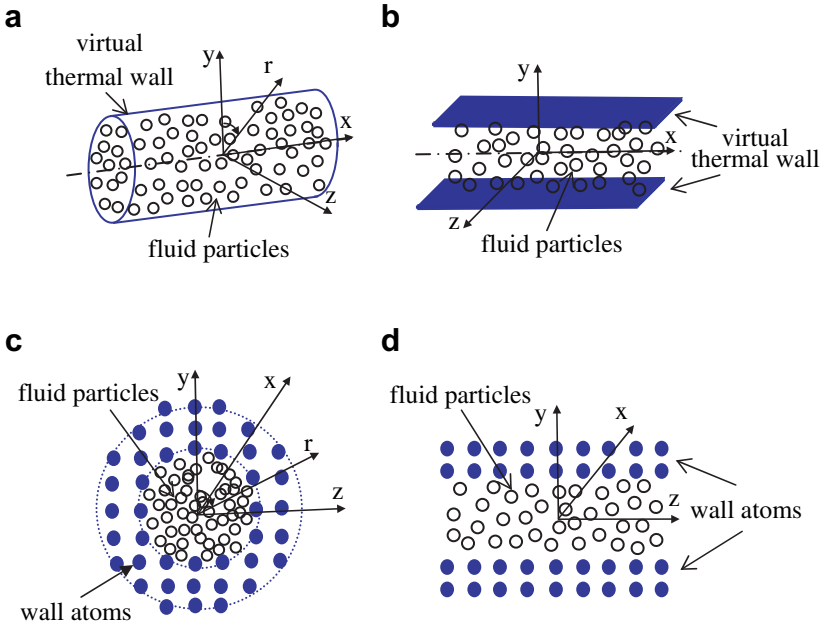

Fig. 1. Simulation geometries for Poiseuille flow: (a) the flow through cylindrical pores with thermal wall model, (b) the flow through slit-like pore with thermal wall model, (c) the flow through cylindrical pores with structured wall model, (d) the flow through slit-like pores with structured wall model. The cylindrical coordinate system is used for cylindrical pores and Cartesian coordinate system for slit-like pores when collecting the data of local properties.

system unchanged, the wall temperature (T_w) is usually fixed at a constant [3,4,8,9,11–15,17] so that the heat can be convected out through the momentum exchange between the fluid and wall. In this work, the wall temperature is kept at 0.8 in non-dimensional unit. The periodic boundary condition (PBC) is applied along the x direction to model the pores of infinite length. For the slit-like pore systems, PBC is also applied in the z direction. The information about the cases studied, the dimensions of the pores and unit cells, and the size of the models is summarized in Table 1.

In all the simulations, the equation of motion is integrated using the Verlet algorithm. A cell subdivision and linked-list approach as described by Rapaport [19] is adopted to improve the computational efficiency in the calculation of intermolecular forces. The flow domain is divided into grids of the same volume. When a steady-state condition is reached, a sampling procedure starts. The information collected in each bin includes the number of particles, and the position and velocity of the particles. The local flow properties are then calculated by averaging these sampled data. The production runs consist of 2×10^7 time steps with a time step of 0.0001τ.

2.1. Thermal wall model

The diagram of the thermal wall systems are illustrated in Fig. 1a and b. In these systems, the pore surfaces are modeled as a continuum with the precise microscopic structures of the walls neglected. When a fluid particle strikes the wall surface, it is assumed to undergo a series of collisions with the surface molecules, and rebound in a randomized velocity, which is uncorrelated with the particle's initial velocity [20,21]. After collisions, the particle leaves the wall surface with a velocity determined by the wall temperature (T_w). The parallel components of the velocity ($v_{//}$)

Table 1
Dimensions of the pores and unit cells, and the size of the models for the cases studied. l_x^*, l_y^*, and l_z^* are the dimensionless edge lengths of the unit cells in x, y, and z direction, respectively. $(l_x^*, l_y^*, l_z^*) = (l_x, l_y, l_z)/\sigma_f$

Case	Pore type	Fluid-wall interaction model	Radius or half-width of the pore	Unit cell dimensions ($l_x^* \times l_y^* \times l_z^*$)	Number of fluid particles	Number of solid atoms
a	Cylindrical	Thermal wall	2.5 σ_f	306.0 × 5.0 × 5.0	4710	n/a
b	Slit-like	Thermal wall	2.5 σ_f	120.0 × 5.0 × 10.0	4697	n/a
c	Cylindrical	Thermal wall	5.0 σ_f	78.0 × 10.0 × 10.0	4786	n/a
d	Slit-like	Thermal wall	5.0 σ_f	60.0 × 10.0 × 10.0	4696	n/a
e	Cylindrical	Structured wall	3.26 σ_f	434.54 × 13.04 × 13.04	6648	35,200
f	Slit-like	Structured wall	3.26 σ_f	435.62 × 11.95 × 11.95	22,055	26,466
g	Cylindrical	Structured wall	5.43 σ_f	173.81 × 17.38 × 17.38	12,538	19,200
h	Slit-like	Structured wall	5.43 σ_f	173.81 × 17.38 × 17.38	15,939	10,626

are chosen by random sampling from the Gaussian distribution, and the normal components ($v_\perp$) are sampled from the probability density [17,21]:

$$f(v_{//}) = \sqrt{\frac{m_f}{2\pi k T_w}} \exp\left[-\frac{m_f v_{//}^2}{2kT_w}\right] \quad (3)$$

$$f(v_\perp) = \frac{m_f}{kT_w}|v_\perp| \exp\left[-\frac{m_f v_\perp^2}{2kT_w}\right] \quad (4)$$

where m_f is the mass of a fluid particle, k the Boltzmann constant. The whole procedure is often called a thermalization process.

During the simulation, when a fluid particle crosses the thermal wall, it is brought back into the pore region via the reentry mechanism as shown in Fig. 2. At time t, a particle j is in position A and is assumed to strike the wall at position B during the time interval $(t,t+\Delta t)$. After the thermalization process, the particle is expected to rebound with the velocity determined from Eqs. (3) and (4), and reach position C at time $t+\Delta t$ [22]. However, the particle is brought to B′ at $t+\Delta t$ owing to the discreteness of the integration algorithm. Here we propose a procedure to bring the particle back to C:

1) Assume that particle j reaches B at $t+\alpha\Delta t$, the coefficient α is less than 1 and can be calculated from $\alpha = |AB|/|AB'|$.
2) Move particle j from B′ to B according to:

$$\vec{r}_j(t+\alpha\Delta t) = \vec{r}_j(t+\Delta t) - (1-\alpha)\Delta t\,\vec{v}(t+\Delta t/2)$$

3) Endow the particle at B with the thermal velocity $\vec{v}_j(t+\alpha\Delta t)$, which is consistent with the distribution expressed in Eqs. (3) and (4).
4) Bring particle j from B to C using the following equation:

$$\vec{r}_{j_{\text{corrected}}}(t+\Delta t) = \vec{r}_j(t+\alpha\Delta t) + (1-\alpha)\Delta t\,\vec{v}_j(t+\alpha\Delta t)$$

2.2. Structured wall model

The structured wall systems are illustrated in Fig. 1c and d. The pore walls are cut out of the bulk solid with the individual atoms arranged in a simple cubic lattice. The lattice length is equal to 1.09 σ_f. Although simple cubic system is rare in nature and only Polonium crystallizes to a simple cubic structure over a limited temperature range, it is a sensible choice for qualitative MD studies as the simplest cubic structure. The models studied here should reveal fundamental phenomena for a wide variety of materials in a computationally economical manner. The interaction between solid atoms also can be modeled with Lennard–Jones potential:

$$\phi_s(d) = 4\varepsilon_s\left[\left(\frac{\sigma_s}{d}\right)^{12} - \left(\frac{\sigma_s}{d}\right)^{6}\right] \quad (5)$$

where σ_s and ε_s are set to be 0.73 σ_f and 50.0 ε_f, respectively. The cut-off distance is 2.5 σ_s. The wall atoms are tethered to its lattice position by a stiff spring with the spring constant set to $2000\varepsilon_s/\sigma_s^2$. During the simulation, a Gaussian thermostat [23] is applied to the solid atoms to maintain the constant wall temperature. The Lennard–Jones potential is also used for the fluid-solid interaction:

$$\phi_{fs}(d) = 4\varepsilon_{fs}\left[\left(\frac{\sigma_{fs}}{d}\right)^{12} - \left(\frac{\sigma_{fs}}{d}\right)^{6}\right] \quad (6)$$

Based on the Lorentz–Berthelog combining rule, σ_{fs} is chosen to be the average of σ_f and σ_s, and ε_{fs} is assumed to be $\sqrt{\varepsilon_f\varepsilon_s}$. The cut-off distance is 2.5 σ_{fs}.

3. Results and discussion

In the NEMD simulations, the fluid domain is divided into 30 bins of the same volume to collect the local data of the number density, velocity and temperature. For cylindrical pores, the division is along the radial direction. The segmental thickness of the bins decreases approaching the pore walls and a high resolution of the data ($<0.09\sigma_f$) is achieved at the interface. For slit-like pores, the division is in the y direction and each bin has the same segmental width. The data collected for the slit-like pores have been symmetrized about the x–z plane to compare with the results for the cylindrical pores.

3.1. Number density profiles

Fig. 3 shows the number density profiles in the cylindrical pores obtained from the thermal wall model. The density has been normalized using the average fluid density of

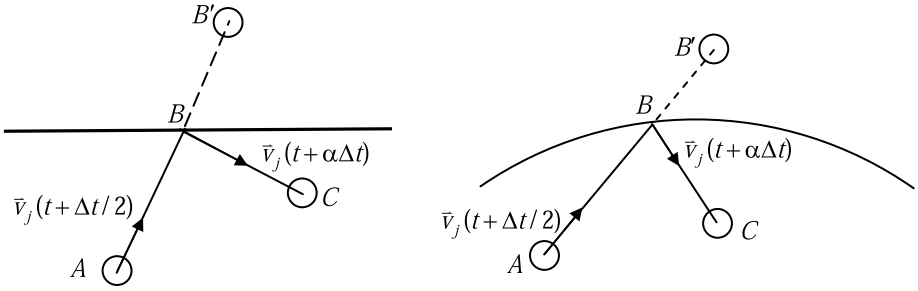

Fig. 2. Reentry mechanism at the thermal wall for the cases of slit-like (left) and cylindrical (right) pores. The reentry path is B′ → B → C.

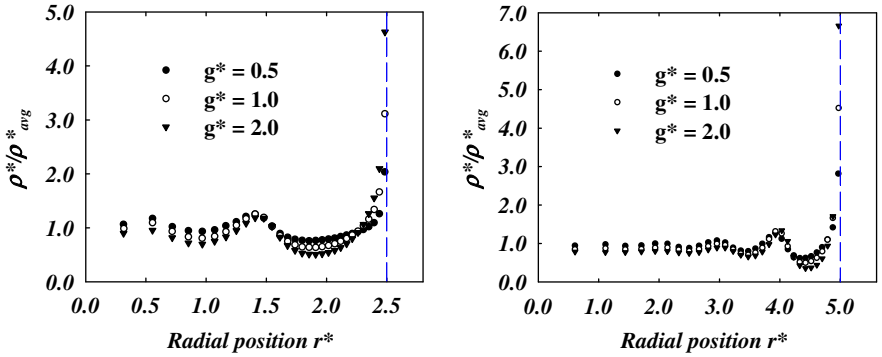

Fig. 3. Radial density profiles of the fluid in the cylindrical pores with the radius of 2.5 σ_f (left) and 5.0 σ_f (right) obtained by the thermal wall model. The dashed line represents the location of the wall.

0.78, and the dimensionless radius $r^* = r/\sigma_f$. The wall is found to disturb the uniform distribution of the fluid particles, and the fluid density oscillates greatly near the wall. The profiles show three peaks near the wall with the magnitudes decreasing with the distance from the wall. It indicates that the wall disturbance weakens and finally dies out at the distance of about $2.85\sigma_f$ (0.97 nm). The effects of the wall disturbance are similar in the two pores of different sizes. The fluid densities in the cylindrical pores are compared with those in slit-like pores of the same sizes. As shown in Fig. 4 with $y^* = y/\sigma_f$, the thermal wall model predicts no significant difference between the density profiles in the two different types of pores. Thus, the single factor of the pore shape does not impose appreciable influence on the fluid density when the molecular interaction between fluid and wall is not considered.

We now examine the effect of molecular interactions at the fluid-wall interface on the fluid density by studying the results from the structured wall model. Fig. 5 compares typical snapshots of the fluid particles and the fluid density profiles in cylindrical and slit-like pores. The radius of the cylindrical pore and the half-width of the slit-like pore are both $5.43\sigma_f$ (1.85 nm), which is the distance between the center line of the pore and the innermost layer of the solid atoms. Due to the strong solid–liquid molecular interactions, the fluid particles are packed orderly at the interface in a pattern consistent with the solid lattice. For the cylindrical pore, fluid particles even penetrate the solid lattice at the four corners. This is due to greater molecular roughness at these locations. When the gravity force (g^*) is 0.5, 1.0 and 2.0, the penetrating fluid particles trapped in the wall pits account for 35%, 29%, and 25% of the total number of fluid atoms, respectively. This leads to a significant decrease of the fluid density in the central region. The increase of the driving force evidently weakens the effect of the wall adsorption, and the fluid density in the central region correspondingly increases. In the slit-like pore, no penetration occurs. Therefore, the fluid density in the central region is almost equal to the average density, and is almost independent of the driving force. The features of the density profile in the slit-like pore are in agreement with most of previous studies [5,8]. Like the results from the thermal wall model, the fluid density oscillates near the wall. Two discernible peaks are observed for both cylindrical and slit-like pores. The interface region, defined as the region where the local density oscillates, has a distance of about $2.50\sigma_f$ (0.85 nm). When the pore size (radius for the cylindrical pore, and half width for the slit-like pore) is decreased to $3.26\sigma_f$ (1.11 nm), steady flow can not be achieved in the cylindrical pore for $g^* \leqslant 2.0$. However,

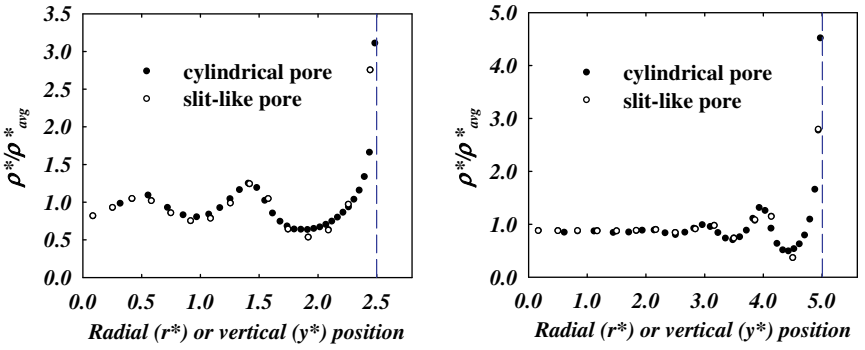

Fig. 4. Comparison of density profiles in cylindrical and slit-like pores obtained by the thermal wall model. The dashed line represents the location of the wall.

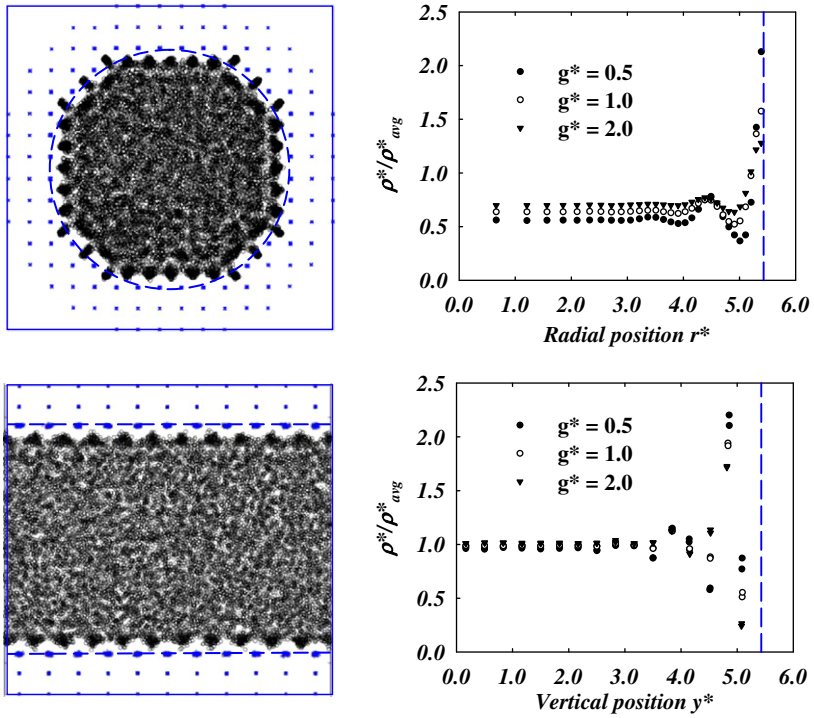

Fig. 5. Snapshots of typical fluid structures and the density profiles in the cylindrical (top) and slit-like (bottom) pores. The radius or half-width of the pore is $5.43\sigma_f$. The dashed line represents the location of the wall.

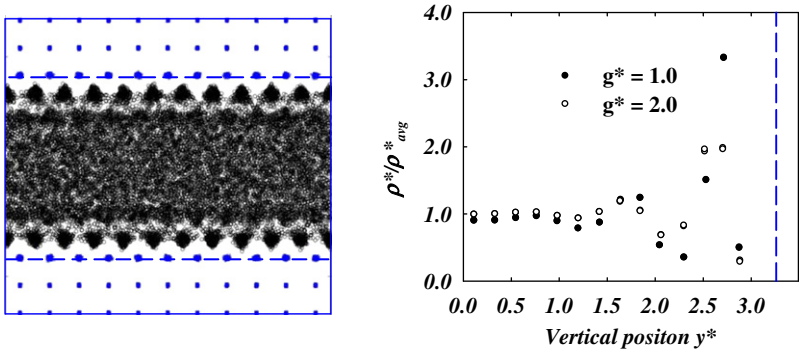

Fig. 6. Snapshots of typical fluid structures and the density profiles in slit-like pore with the half-width of $3.26\sigma_f$. The dashed line represents the location of the wall.

the steady flow is developed in the slit-like pore when g^* is equal to 1.0 and 2.0. The snapshot of the simulation system and the fluid density are illustrated in Fig. 6.

The thermal wall model predicts that the density of the fluid layer nearest the wall significantly increases with the magnitude of the external force although the overall density profiles just vary slightly (see Fig. 3). This is related with the reentry mechanism used in the thermal wall model. When a larger gravity force is applied, the thermal motion of the fluid particles is enhanced as a result of increased kinetic energy. This leads to the increase in the probability of the fluid particle-wall collisions. Therefore, a larger number of fluid particles strike the wall and are brought back to the locations nearest the wall by the reentry mechanism. The phenomenon is not observed in the results from the structured wall model, and it could be artificial and induced by the stochastic procedure in the thermal wall model.

3.2. Flow velocity profiles

At macroscale, the flow velocity profile in the cylindrical pore is similar to that in the slit-like pore. With the assumptions of no slip and uniform state variables of density and temperature, the streaming velocity of the flow (v_x) in the two types of pores can be obtained by solving Navier–Stokes equations:

$$v_x = -\frac{1}{4}\frac{\rho g}{\eta}(r^2 - a^2) \text{ in cylindrical pores}$$
$$v_x = -\frac{1}{2}\frac{\rho g}{\eta}(y^2 - a^2) \text{ in slit-like pores} \quad (7)$$

where ρ and η are the density and viscosity of the fluid, respectively; a represents the radius of the cylindrical pore and the half-width of the slit-like channel.

Figs. 7–9 compare the dimensionless streaming velocity in the x direction for the nanoscale cylindrical and slit-like channels, and Fig. 10 shows the velocity profile in the slit-like pore with $a = 3.26\sigma_f$ obtained from the structured wall model. In these figures, the simulation results are represented by symbols, and the solid lines are quadratic curves fitted from the data. Figs. 7 and 10 show that the velocity profiles deviate from the quadratic curves when the pore size is small. They possess an underlying quadratic signature with superimposed oscillation in the region near the wall. When increasing the pore size (see Figs. 8 and 9), the velocity profiles become closer to the quadratic curves although large oscillation is still present for the case of $g^* = 2.0$. Therefore, the oscillation in the velocity near the wall might be attributed to the small size of the confinement and large external force. The velocity profiles in the cylindrical and slit-like pores have the same trend, but the slip behaviors at the interfaces are quite different in the two types of nanochannels. As shown in Fig. 9, slip on the boundary is evident in the cylindrical pore while no slip is observed at the interface for the slit-like pore.

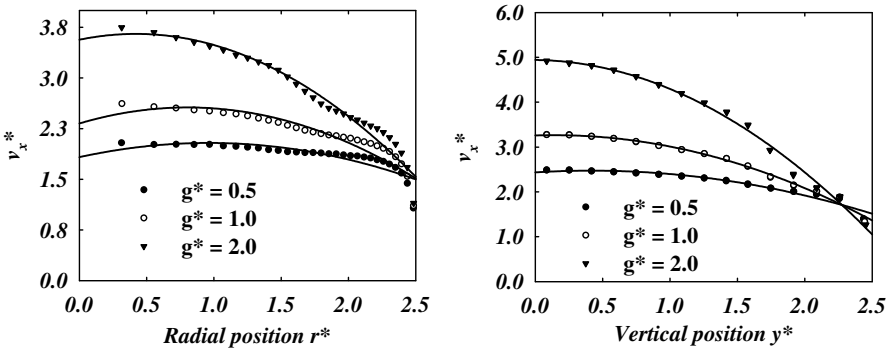

Fig. 7. Streaming velocity profiles in the cylindrical (left) and slit-like (right) pores obtained by the thermal wall model. The radius or half-width of the pore is $2.5\sigma_f$.

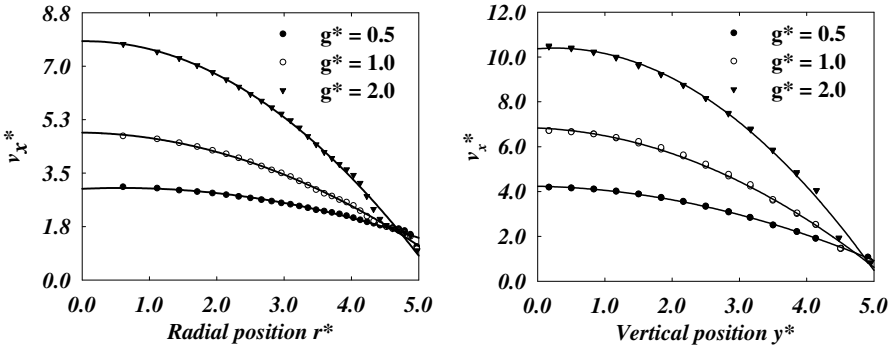

Fig. 8. Streaming velocity profiles in the cylindrical (left) and slit-like (right) pores obtained by the thermal wall model. The radius or half-width of the pore is $5.0\sigma_f$.

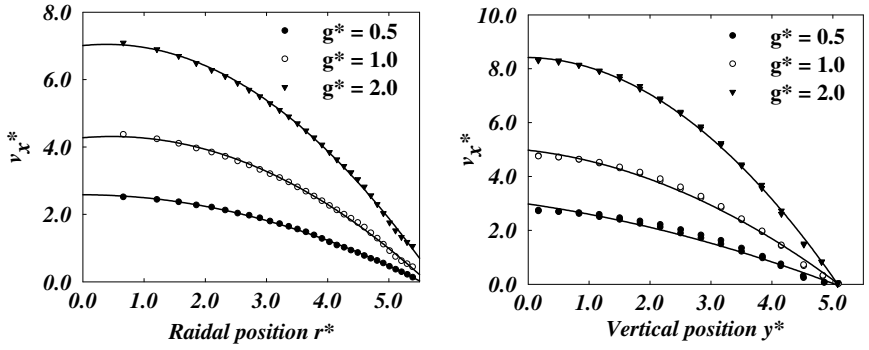

Fig. 9. Streaming velocity profiles in the cylindrical (left) and slit-like (right) pores obtained by the structured wall model. The radius or half-width of the pore is $5.43\sigma_f$.

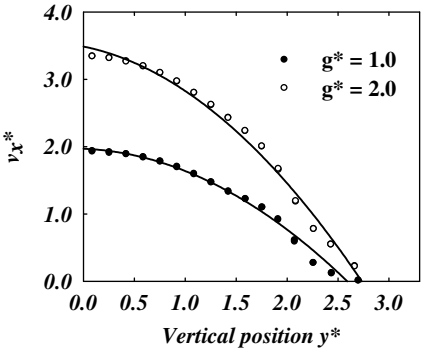

Fig. 10. Streaming velocity profiles in the slit-like pore with the half width of $3.26\sigma_f$obtained by the structured wall model.

When $g^* = 0.5$, 1.0, and 2.0, the slip length for the cylindrical pore is found to be $0.085\sigma_f$, $0.21\sigma_f$, and 0.34 σ_f, respectively. The slip length is calculated by extrapolating the velocity profile to where the velocity would vanish within the solid. As reported by other researchers [5,11], the slip length increases with the external driving force.

3.3. Temperature profiles

The dimensionless temperature T^* at the mass center of each bin can be calculated from

$$T^* = \frac{1}{N}\sum_{n=1}^{N}\frac{2}{3}\sum_{i=1}^{3}\frac{1}{2}\left(v_{n,i}^* - \frac{1}{N}\sum_{m=1}^{N}v_{m,i}^*\right)^2 \tag{8}$$

where N is the number of fluid particles in the bin, and $v_{n,i}^*(= v_{n,i}\sqrt{m_f/\varepsilon_f})$ is the non-dimensionalized velocity of molecule n in the i (=x, y, z) direction. The steady-state temperature profiles are time-averaged data sampled during the production run.

The temperature profiles of the fluid in the cylindrical pores are compared with those in the slit-like pores of the same size in Figs. 11–14 show the temperature profile predicted by the structured wall model in the slit-like pore with the radius of $3.26\sigma_f$. The actual values of the temperature in Figs. 11,13 and 14 can easily be converted from the dimensionless T^* according to Eq. (2). Both the thermal wall and structured wall models predict lower temperature and more uniform temperature distribution in the cylindrical pores. The better performance of the cylindrical pores to conduct the viscous heat out of the channels could be attributed to the following factors: (1) the surface-to-volume ratio of the cylindrical pores is twice that of the slit-like pores of the same characteristic size. Therefore, a larger number of surface particles participate in the momentum exchange between the fluid and wall; (2) the curvature and greater molecular roughness in the cylindrical pores further enhance the molecular interaction between the fluid and

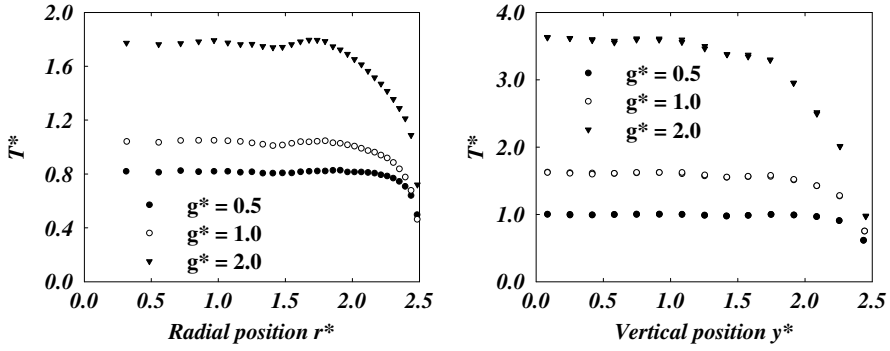

Fig. 11. Temperature profiles in the cylindrical (left) and slit-like (right) pores obtained by the thermal wall model. The radius or half width of the pore is $2.5\sigma_f$.

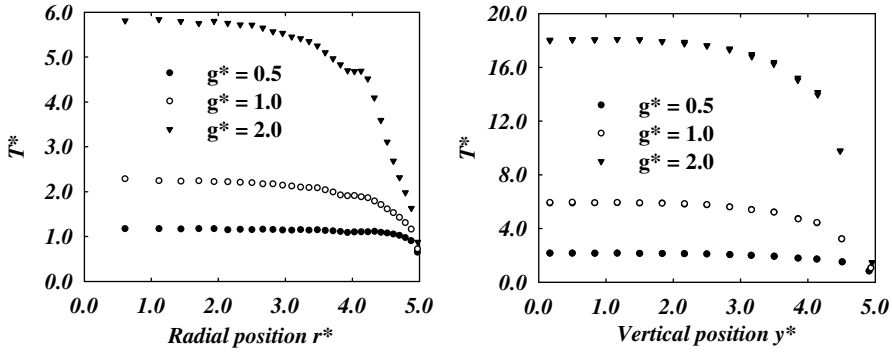

Fig. 12. Temperature profiles in the cylindrical (left) and slit-like (right) pores obtained by the thermal wall model. The radius or half width of the pore is $5.0\sigma_f$.

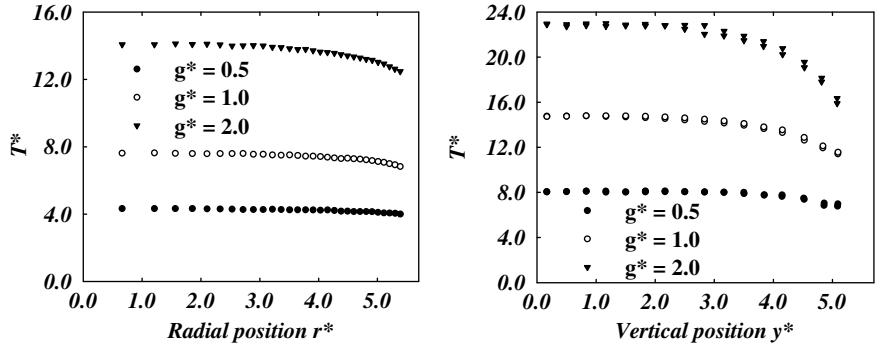

Fig. 13. Temperature profiles in the cylindrical (left) and slit-like (right) pores obtained by the structured wall model. The radius or half width of the pore is $5.43\sigma_f$.

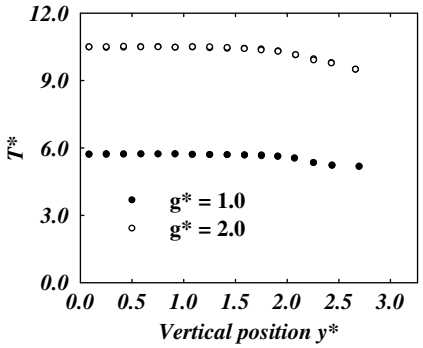

Fig. 14. Temperature profiles in the slit-like pore with the half-width of $3.26\sigma_f$ obtained by the structured wall model.

wall atoms. It also shows that narrower pores perform better to remove the viscous heat as a result of larger surface-to-volume ratio and greater curvature.

The results in Figs. 11 and 12 illustrate that the thermal wall model predicts lower fluid temperature when compared to the structured wall model. The thermal wall model modifies the velocity of the fluid particles colliding with the wall and imposes the low temperature of the wall onto the fluid layer near the wall. This procedure lowers the temperature of the fluid in the whole channel. On the other hand, the fluid temperature computed by the structured wall model is high and there exists a large temperature jump at the fluid-wall interface. It indicates an insufficient thermal coupling between the wall and fluid momenta and might be related with the large driving force. The large temperature jump at the interface is also reported in other molecular dynamics studies [3,24]. Further studies are necessary to investigate the cause of the phenomenon, and a more accurate model for the fluid-wall interaction might be needed.

4. Conclusions

Nonequilibrium molecular dynamics simulations are performed to investigate the gravity force driven Poiseuille flow in nanochannels of different sizes. Two different models (the thermal wall and structured wall model) are adopted to model the fluid-wall interaction. The effect of the pore shape on the nanoscale Poiseuille flow is also studied by comparing the fluid behaviors through cylindrical and slit-like pores of the same confinement size. The following conclusions are drawn from the present study:

1. In both cylindrical and slit-like nanochannels, the fluid density varies appreciably near the solid wall surface. The single factor of the pore shape does not impose significant influence on the fluid density. However, the computer experiment of carving the pores out of the solid lattice yields the cylindrical pores with larger molecular corrugation than the slit-like pores. Thus, a larger number of fluid particles appose onto the wall surface and it results in a much lower bulk fluid density in the cylindrical pores. In the engineering practice, a smooth flat surface is also easier to be produced than the curved surface with the same grade of surface smoothness. On the other hand, the atoms on the surface should rearrange and form the structure different from the bulk lattice. This rearrangement process should be dependent of the pore shape, and yields surfaces of different roughness. Therefore, the phenomenon observed in the simulation might be of practical concern for the design of nanodevices.
2. The streaming velocity profiles in the two different types of pores have the same quadratic or close-to-quadratic trend, but larger slip on the boundary is observed in the cylindrical pore. The flow velocity depends on the driving force, and the density and viscosity of the fluid. In nanoscale, the effect of the pore shape and size on the state variables of the fluid is complicated. Further studies are needed to identify the relationship between the velocity, the flow resistance of the fluid, driving force, pore shape, and pore size.
3. There exists a stronger fluid-wall interaction in cylindrical nanopores than in slit-like nanochannels due to larger surface-to-volume ratio, curvature, and possibly greater molecular roughness. Therefore, the cylindrical pores perform better to conduct the viscous heat out of channel. The fluid temperature in the cylindrical pores is lower than the slit-like pores of the same size. The fluid

temperature decreases with the pore size as a result of increasing surface-to-volume ratio and curvature.

4. Thermal wall model does not include the molecular interaction between the fluid and wall atoms, and therefore can not accurately predict the fluid structure at interface, the fluid density variation, and slip phenomenon on the boundary. However, the streaming velocity and temperature predicted by the thermal wall model agree with the results from the structured wall model qualitatively.

References

[1] C. Neto, D.R. Evans, E. Bonaccurso, H. Butt, V.S.J. Craig, Boundary slip in Newtonian liquids: a review of experimental studies, Rep. Prog. Phys. 68 (2005) 2859–2897.

[2] M. Gad-el-Hak, Liquids: the holy grail of microfluidic modeling, Phys. Fluids 17 (2005) 100612.

[3] K.P. Travis, K.E. Gubbins, Poiseuille flow of Lennard–Jones fluids in narrow slit pores, J. Chem. Phys. 112 (2000) 1984–1994.

[4] K.P. Travis, B.D. Todd, D.J. Evans, Departure from Navier–Stokes hydrodynamics in confined liquids, Phys. Rev. E 55 (1997) 4288–4295.

[5] G. Nagayama, P. Cheng, Effects of interface wettability on microscale flow by molecular dynamics simulation, Inter. J. Heat Mass Transfer 47 (2004) 501–513.

[6] M. Cieplak, J. Koplik, J.R. Banavar, Boundary conditions at a fluid-solid interface, Phys. Rev. Lett. 86 (2001) 803–806.

[7] J.-L. Barrat, L. Bocquet, Large slip effect at a nonwetting fluid-solid interface, Phys. Rev. Lett. 82 (1999) 4671–4674.

[8] S.A. Somers, H.T. Davis, Microscopic dynamics of fluids confined between smooth and atomically structured solid surfaces, J. Chem. Phys. 96 (1992) 5389–5407.

[9] A. Jabbarzadeh, J.D. Atkinson, R.I. Tanner, J. Chem. Phys. 110 (1999) 2612–2620.

[10] P.A. Thompson, S.M. Troian, A general boundary condition for liquid flow at solid surfaces, Nature 389 (1997) 360–362.

[11] J.L. Xu, Z.Q. Zhou, Molecular dynamics simulation of liquid argon flow at platinum surfaces, Heat Mass Transfer 40 (2004) 569–859.

[12] X.-B. Mi, A.T. Chuang, Molecular dynamics simulations of nano-channel flows at low Reynolds numbers, Molecules 8 (2003) 193–206.

[13] X.-J. Fan, N. Phan-Thien, N.T. Yong, X. Diao, Molecular dynamics simulation of a liquid in a complex nano channel flow, Phys. Fluids 14 (2002) 1146–1153.

[14] S.K. Bhatia, D. Nicholson, Hydrodynamic origin of diffusion in nanopores, Phys. Rev. Lett. 90 (2003) 016105.

[15] O.G. Jepps, S.K. Bhatia, D.J. Searles, Wall mediated transport in confined spaces: exact theory for low density, Phy. Rev. Lett. 91 (2003) 126102.

[16] S.K. Bhatia, O. Jepps, D. Nicholson, Tractable molecular theory of transport of Lennard–Jones fluids in nanopores, J. Chem. Phys. 120 (2004) 4472–4485.

[17] H. Kim, C.H. Cho, E.K. Lee, Dynamics of simple fluids confined in cylindrical pore: effect of pore size, J. Theo. Comp. Chem. 4 (2005) 305–315.

[18] V.P. Sokhan, D. Nicholson, N. Quirke, Fluid flow in nanopores: accurate boundary conditions for carbon nanotubes, J. Chem. Phys. 117 (2002) 8531–8539.

[19] D.C. Rapaport, The Art of Molecular Dynamics Simulation, 2nd ed., Cambridge University Press, Cambridge, United Kingdom, 2004.

[20] J.C. Maxwell, Philos. Trans. R. Soc. London Ser. A 170 (1867) 231.

[21] R. Tehver, F. Toigo, J. Koplik, J.R. Banavar, Thermal walls in computer simulations, Phys. Rev. E 57 (1998) R17–R20.

[22] A. Tenenbaum, C. Giovanni, R. Gallico, Stationary nonequilibrium states by molecular dynamics – Fourier's law, Phys. Rev. A 25 (1982) 2778–2787.

[23] D. Brown, J.H.R. Clarke, A comparison of constant energy, constant temperature and constant pressure ensembles in molecular dynamics simulations of atomic liquids, Mol. Phys. 51 (1984) 1243–1252.

[24] B.D. Todd, D.J. Evans, Temperature profile for Poiseuille flow, Phys. Rev. E 55 (1997) 2800–2807.